Journal of Magnetism and Magnetic Materials 503 (2020) 166531

Contents lists available at ScienceDirect

Journal of Magnetism and Magnetic Materials

journal homepage: www.elsevier.com/locate/jmmm

Research articles

Assessment of the critical behavior near the FM to PM phase transition in cubic $Ni_{0.3-x}Cu_xZn_{0.7}Fe_2O_4$ spinel ferrite

R. Felhi[a,*], K. Riahi[a,b], H. Omrani[a], M. Koubaa[c], W. Cheikhrouhou Koubaa[a], A. Cheikhrouhou[a]

[a] Laboratoire des Technologies des Systèmes Smarts (LT2S), Centre de Recherche Numerique Sfax, Cité El Ons, Route de Tunis, Km 9, Sfax, B.P. 275, Sakiet Ezzit, 3021 Sfax, Tunisia

[b] Magnetic Detection and Imaging Group (MD&I), University of Twente, Enschede, the Netherlands

[c] Institut Supérieur de Biotechnologie de Sfax, Université de Sfax, B.P 261, 3000 Sfax, Tunisia

ARTICLE INFO

Keywords:
Zn-Ni-Cu ferrites
Crystal structure
Morphology
Critical behavior

ABSTRACT

In this study, we report a thorough examination of the critical behavior of the cubic $Ni_{0.3-x}Cu_x$ $Zn_{0.7}Fe_2O_4$ (x = 0.0, 0.1 and 0.2) spinel ferrite which are crystallized with different irregular shapes of particle size (spherical,polygonal and cubic). The magnetic transition is ferromagnetic to paramagnetic state for all Cu-doped compounds. Different theoretical analyses, as the modified Arrott plot, Kouvel–Fisher method, and critical isotherm, have been used to identify the values of the ferromagnetic transition temperature T_C, and the critical exponents of β, γ and δ. All the obtained values of critical parameters were found to be close to the 3D-Heisenberg theoretical model, which implies short-range magnetic interactions in Cu-doped compounds. The reliability of critical parameters was further checked through different methods, such as the Widom scaling relationship and the magnetic equation.

1. Introduction

The spinel ferrites ceramics with the general formula MFe_2O_4 (where M^{2+} = Mn^{2+}, Co^{2+},Cd^{2+}, Fe^{2+}, Ni^{2+}, Cu^{2+}, Zn^{2+} etc…) are an important class of technological materials thanks to their excellent electrical and magnetic properties. Their properties depend strongly on their chemical composition, cation distribution, technique of preparation in general and structure in particular [1]. They have been largely used in several applications, such as in high-density magnetic recording, microwave devices, and magnetic fluids [2–4]. Indeed, few studies with these materials have also been found to exhibit the large magnetocaloric effect (MCE) under a moderate applied magnetic field revealing that these compounds are possible candidates for magnetic refrigeration applications [5–9]. Despite this large MCE, it remains the problem with the very high Curie temperatures of ferrites that limit its use in magnetic refrigeration near room-temperature (~300 K). Thanks to chemistry, the Curie temperature T_C can be adjusted by proper ions doping. As noted in the work conducted by M. S. Anwar et al. [6] the substitution of Ni by non-magnetic Zn in $Ni_{1-x}Zn_xFe_2O_4$ mixed ferrites, resulting in a large shift in T_C from 845 K to 302 K as x varied between 0.0 and 0.7.Moreover, Shahida Akhter et al. [7] have reported that doping with a non-magnetic element Zn leads to a drop of T_C in $Cu_{1-x}Zn_xFe_2O_4$ ferrites from 373 to 140 K for x = 0.6 and 0.8 respectively. As we see, we could easily adjust and tune the temperature for each application, which is very beneficial for operating magnetic refrigeration in various temperature ranges. Therefore, it has been attracted much attention to systematically adjust the magnetic properties of spinel ferrites either by changing the divalent cation or by a partial substitution. Accordingly, after we have studied the effect of copper (Cu) doping level in $Zn_{0.7}Ni_{0.3-x}Cu_xFe_2O_4$ ($0 \le x \le 0.2$) system in our previous work [10], we succeeded in improving their magnetocaloric response around room temperature.

The analysis of the MCE of ferrite materials is significant not only has it a potential application perspective, but also because it is considered as a means that can help to understand the intrinsic properties of ferrites. Specially, the details of the magnetic phase transition and critical behavior can be obtained through the MCE. In fact, the analysis of the critical behavior in the vicinity of the magnetic phase transition is a powerful tool that helps analyze in details the mechanisms of the magnetic interaction responsible for the transition [11,12]. Magnetic particles are classified by their magnetic interactions into four models, 'the Mean field', 'the 3D-Heisenberg', 'the 3D-Ising' and 'the tricritical mean- field'. Each theoretical model has its own critical exponents values β, γ and δ. For the mean-field (β = 0.5, γ = 1 and δ = 3), the 3D-Heisenberg (β = 0.365, γ = 1.336 and δ = 4.80), the 3D-Ising (β = 0.325, γ = 1.241 and δ = 4.82), and the tricritical mean-field

* Corresponding author.
E-mail address: ramzifelhi88@gmail.com (R. Felhi).

https://doi.org/10.1016/j.jmmm.2020.166531
Received 6 July 2019; Received in revised form 30 December 2019; Accepted 29 January 2020
Available online 01 February 2020
0304-8853/

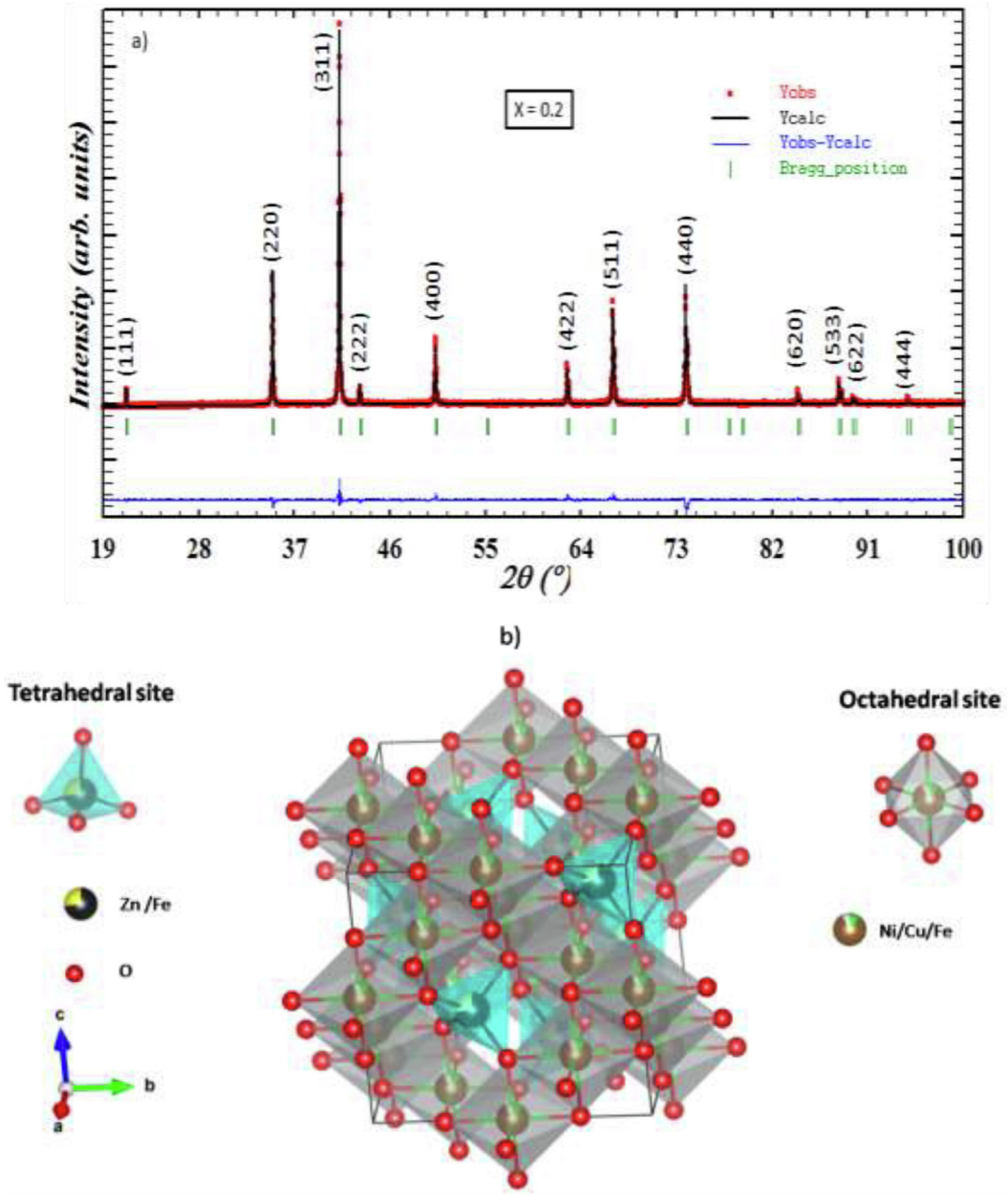

Fig.1. (a) XRD patterns for the $Ni_{0.1}Cu_{0.2}Zn_{0.7}Fe_2O_4$ compound. (b) The unit cell of the $Ni_{0.1}Cu_{0.2}Zn_{0.7}Fe_2O_4$ ferrite spinel structure generated by VESTA program.

($\beta = 0.25$, $\gamma = 1$ and $\delta = 5$) models [13].

As we mention above, we have prepared elsewhere the cubic $Ni_{0.3-x}Cu_x$ $Zn_{0.7}Fe_2O_4$ (x = 0.0, 0.1 and 0.2) spinel ferrite [10]. To fully understand their magnetic interaction, we need to pursue our work with the detail of the critical phenomena near the ferromagnetic (FM) – paramagnetic (PM) phase transition, which is the purpose of this paper.

2. Experimental details

Ferrite compounds of the chemical formula $Ni_{0.3-x}Cu_x$ $Zn_{0.7}Fe_2O_4$ ($0.0 \leq x \leq 0.2$) are prepared using the sol–gel method described previously [10]. All materials crystallize in the cubic structure with $Fd\bar{3}m$ space group. The morphology of the compounds was observed with a scanning electron microscope (SEM). Magnetic measurements were performed by vibrating sample Magnetometer (VSM) J3590 mini CFM of Cryogenics.

3. Results and discussion

The X-ray diffraction (XRD) patterns of the $Ni_{0.1}Cu_{0.2}$ $Zn_{0.7}Fe_2O_4$ (x = 0.2) compound as well as the Miller index are shown in Fig. 1 a. A single phase material is observed without any detectable impurity. All the $Ni_{0.3-x}Cu_x$ $Zn_{0.7}Fe_2O_4$ compounds are crystallized in cubic system with Fd-3m space group [10]. Also, the unit cell volume increases upon Cu^{2+} doping, which indicates that Cu^{2+} ions have been entered successfully into the lattice of the Zn-$NiFe_2O_4$. The increasing trend of the unit cell volume is attributed to the substitution of smaller ionic size of Ni^{2+} (0.69 Å) by the larger ionic size of Cu^{2+} (0.72 Å) in the host system. To understand the structure and distribution of Zn/Ni/Cu/Fe ions on two available Crystallographic (A site and B sites) and oxygen positions of materials, the systematic crystal structure is generated using a. cif file from X-ray diffraction refinement by VESTA program. The unit cell for $Ni_{0.1}Cu_{0.2}Zn_{0.7}Fe_2O_4$ (x = 0.2) compound is displayed in Fig. 1b. Indeed, it is well described with cubic structure, closely packed, with two interstitial sites, the tetrahedral (A) and octahedral

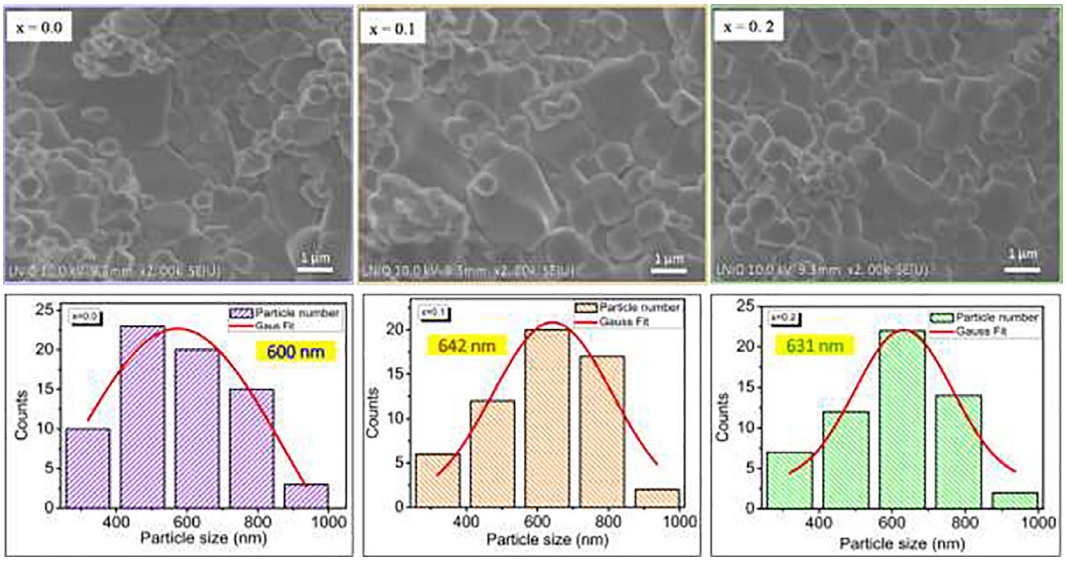

Fig.2. SEM images of the $Ni_{0.3-x}Cu_x$ $Zn_{0.7}Fe_2O_4$ ($0.0 \leq x \leq 0.2$) ferrite.

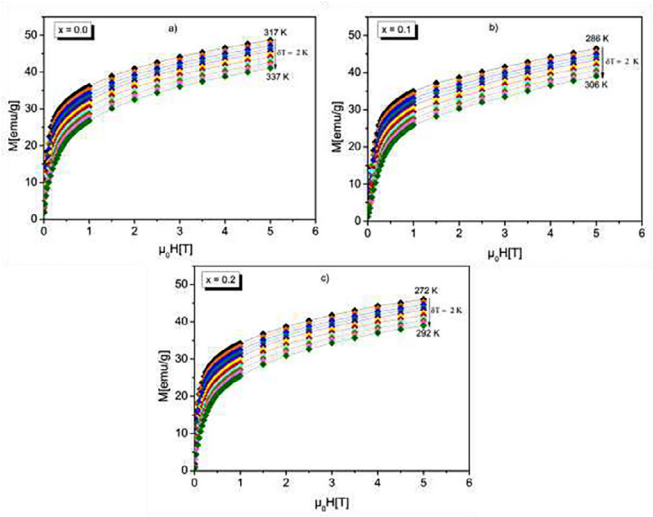

Fig.3. Isothermal magnetization for $Ni_{0.3-x}Cu_x$ $Zn_{0.7}Fe_2O_4$ for (a) x = 0.0 (b) x = 0.1 and (c) x = 0.2 measured at different temperatures around T_C.

(B) sites which are surrounded by four and six oxygen ions. The tetrahedral site, in which Zn/Fe atom is situated amidst four oxygen atoms which form the corners of a regular tetrahedron and the octahedral site where, Ni/Cu/Fe atom is situated in the middle of the six oxygen atoms forming the corners of a regular octahedron are well displayed in the crystal structure.

The morphology and particle size of our compounds, revealed by scanning electron microscopy (SEM), are shown in Fig. 2. These micrographs show that the prepared spinel ferrites have a several irregular shapes (spherical, polygonal, cubic…). It is important to mention that different regions are selected to analyze the particle sizes and around 50 particles are measured. For that, a manual statistical count of particle size has been performed on MEB images using the Image-J software. The results are expressed in Fig. 2 as particle number (counts) vs. particle size (nm). These particles were distributed, for the $Ni_{0.3-x}Cu_x$ $Zn_{0.7}Fe_2O_4$ (x = 0.0, 0.1 and 0.2) compounds, according to a Gaussian function (red solid line). The obtained values of particle sizes are 600, 642 and 631 nm for x = 0.0, 0.1 and x = 0.2, respectively, which are greater than the average crystallite size determined by XRD [10]. This can be ascribed to the fact that each particle observed by SEM is formed by several crystallites [14].

The temperature dependence of magnetization at an applied field of 0.05 T for $Ni_{0.3-x}Cu_x$ $Zn_{0.7}Fe_2O_4$ ($0.0 \leq x \leq 0.2$) compounds has been reported in our previous work [10]. The M(T) curves showed a PM-FM transition at T_C. The value of T_C was reduced upon Cu^{2+} doping. The decreased of the transition temperature T_C can be interpreted in terms of the decrease in the magnetization of B sublattice in the Cu^{2+} doped compounds.

As mention in several papers [15,16], the critical exponents, β, γ and δ are the spontaneous magnetization(M_S), the inverse of initial susceptibility (χ_0^{-1}) and δ the critical magnetization isotherm (at T_C), respectively [15].They can be described as follows [16]:

$$M_S(T) = M_0(-\varepsilon)^{\beta}, \quad \varepsilon < 0 \tag{1}$$

$$\chi_0^{-1}(T) = \left(\frac{h_0}{M_0}\right)\varepsilon^{\gamma}, \quad \varepsilon > 0 \tag{2}$$

$$M = D(\mu_0 H)^{\frac{1}{\delta}}, \quad \varepsilon = 0 \tag{3}$$

where M_0, $\left(\frac{h_0}{M_0}\right)$ and D are the critical amplitudes, $\varepsilon = \left(\frac{T - T_C}{T_C}\right)$ is the reduced temperature and β, γ and δ are the critical exponents.

Fig. 3 emphasizes the variation of magnetization $M(\mu_0 H, T)$ curves around T_C with step of 2 K for $Ni_{0.3-x}Cu_x$ $Zn_{0.7}Fe_2O_4$ (x = 0.0, 0.1 and 0.2). The magnetization increases steadily with increasing applied magnetic field. The isothermal plots ($M^{\frac{1}{\beta}}$ vs.$\left(\frac{\mu_0 H}{M}\right)^{\frac{1}{\gamma}}$ for our compounds (x = 0.0 and × = 0.2) according to the mean field theory (β = 0.5 and γ = 1) have been plotted in Fig. 4(a and b). The positive slope of these curves reflects that all the compounds presented a second order ferromagnetic (FM) - paramagnetic (PM) phase transition. According to the mean field model, such curves should give a series of straight lines in the high field region at different temperatures, while the line at T_C should cross the origin [17]. From Fig. 4(a and b) that these conditions are not accurate for our compounds revealing that the long-range interaction and the mean- field theory are not satisfied.

Therefore, around the critical temperature, these plots may be modified by choosing trial exponents β and γ from among the above models (the 3D-Heisenberg, 3D-Ising and tri-critical mean-field models) to find the correct values of T_C, spontaneous magnetization $M_S(0, T)$ below T_C, and initial susceptibility $\chi_0(T, 0)$. Thus, we have used the modified Arrott plots (MAP) in order to correctly identify the critical exponents for our compounds based on the so-called Arrot-Noakes equation state [18]. This method is based on the equation of state:

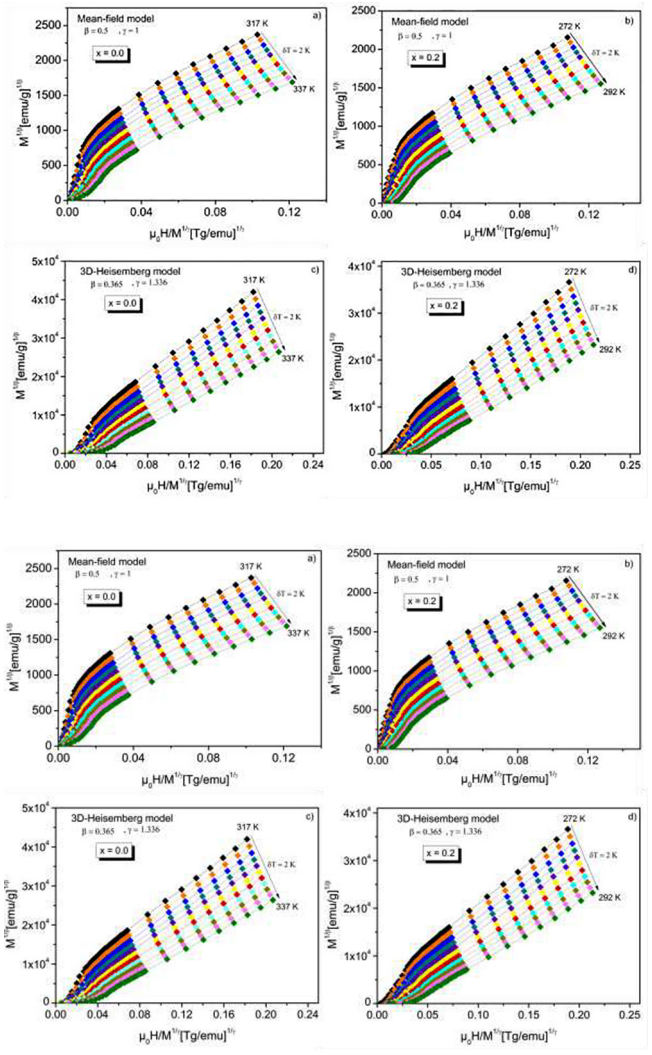

Fig. 4. (a) and (b) Arrott plots around T_C for $Ni_{0.3-x}Cu_x$ $Zn_{0.7}Fe_2O_4$ (x = 0.0 and 0.2). According to the mean field model (values of critical exponents β = 0.5 and γ = 1). Modified Arrott plots (MAP) for x = 0.0 and x = 0.2: isotherms of $M^{1/\beta}$ vs. $(\mu_0H/M)^{1/\gamma}$ with (c) and (d) 3D-Heisenberg model (β = 0.365, γ = 1.336); (e) and (f) 3D-Ising model (β = 0.325, γ = 1.24); (g) and (h) tricritical mean- field model (β = 0.25, γ = 1.0) and as a function of temperature.

$$\left(\frac{\mu_0 H}{M}\right)^{\frac{1}{\gamma}} = a\frac{(T - T_C)}{T} + bM^{\frac{1}{\beta}} \tag{4}$$

where a and b are considered to be constants.

Fig. 4 shows the MAP at different temperatures uses three models of critical exponents for $Ni_{0.3-x}Cu_x$ $Zn_{0.7}Fe_2O_4$ (x = 0.0 and 0.2) compounds: the 3D-Heisenberg model (β = 0.365, γ = 1.336) in Fig. 4 c and d); the 3D-Ising model (β = 0.325, γ = 1.24) in Fig. 4 e and f and the tricritical mean-field model (β = 0.25, γ = 1) in Fig. 4 g and h. One can see that all models yield quasi straight lines and nearly parallel in the high field region. So, it becomes difficult to compare these results and select the best model. For this reason, we calculated their relative slopes (RS) which are defined at the critical point as $RS = \frac{S(T)}{S(T_C)}$, where S (T) and $S(T_C)$ are the slope for a given temperature close to T_C and the slope at $T = T_C$, respectively. The RS of the most appropriate model should be kept to 1 (unity) irrespective of temperatures [19]. As shown in Fig. 5, we can deduce that, for all compounds, the 3D-Heisenberg model is the best one, which can be considered to describe our system and determine the critical exponents. Based on the description mentioned above, we have chosen the initial values of this model's critical exponents (β = 0.365, γ = 1.336) for our compounds. The spontaneous magnetization, $M_S(0.\ T)$, as well as the inverse initial susceptibility, $\chi_0^{-1}(T, 0)$, were determined from the intersections of the linear extrapolation line with the$(M^{\frac{1}{\beta}})$ and the $\left(\frac{\mu_0 H}{M}\right)^{\frac{1}{\gamma}}$ axis, respectively. New β, γ and T_C values was determined from the power-law fitting of $M_S(0.\ T)$ and $\chi_0^{-1}(T, 0)$ curves (Fig. 6 a and b) for $Ni_{0.3-x}Cu_xZn_{0.7}Fe_2O_4$ (x = 0.0 and 0.2) compounds using Eqs. (1) and (2). Similarly, we can also determine $M_S(0.\ T)$ and $\chi_0^{-1}(T, 0)$ for the samples x = 0.1 (not shown here).

In order to obtain accurate critical exponents, the Kouvel-Fisher method has been used on the basis of the following relationship [20]:

$$M_S(T)\left[\frac{dM_S(T)}{d(T)}\right]^{-1} = \frac{T - T_C}{\beta} \tag{5}$$

$$\chi_0^{-1}(T)\left[\frac{d\chi_0^{-1}(T)}{d(T)}\right]^{-1} = \frac{T - T_C}{\gamma} \tag{6}$$

According to these equations, using the obtained $M_S(T)$ and $\chi_0^{-1}(T)$ vs. T from Fig. 6a and b, the plotting of $M_S(T)\left[\frac{dM_S(T)}{d(T)}\right]^{-1}$ and $\chi_0^{-1}(T)\left[\frac{d\chi_0^{-1}(T)}{d(T)}\right]^{-1}$ against temperature in Fig. 6c and d, yields straight lines with slope $\frac{1}{\beta}$ and$\frac{1}{\gamma}$, respectively, and the intercepts on the T axis are equal to T_C. In fact, the linear curves confirm the applicability of Kouvel–Fisher formalism in the current investigation. From the fitted straight lines according respectively to Eqs. (5) and (6), we can carry out the critical exponents and T_C. The obtained results are in agreement with those determined from the modified Arrott plots. The obtained results of the critical exponents and T_C are in agreement with those determined from the modified Arrott plots.

Our critical exponents values for different methods (MAP and KF), some other spinel ferrites compounds found in literature [9,21,22], and the values different theoretical models [10], are given in Table 1 for comparison. From this table, we can see clearly that the values of critical exponents found for the compounds $Ni_{0.3-x}Cu_xZn_{0.7}Fe_2O_4$ (x = 0.0, 0.1 and 0.2) fit with the 3D-Heisenberg-like ferromagnet. Recently, an investigation of critical behavior in $Zn_{0.6-x}Ni_xCu_{0.4}Fe_2O_4$ compounds has been carried out by Elaa Oumezzine et al. [5]. The critical exponents change from the 3D-Heisenberg model for x = 0.0 compound to unconventional exponents for x = 0.2 and 0.4 compounds explained by the substitution of Zn^{2+} (non-magnetic ions) by Ni^{2+} (magnetic ions).

Regarding the values of the exponent δ associated with the isotherms at$T \approx T_C$, it can be obtained by fitting the$M(\mu_0 H, T_C)$. Fig. 7 shows critical isotherms M (T_C) vs. $\mu_0 H$ plots for × = 0.0 and x = 0.2 respectively, and in the insets are the same plots presented in the logarithmic scale. According to Eq. (3), the linear fit of the data at high-fields region should be a straight line with a slope of 1/ δ. From the linear fitting in the insets, we have obtained δ = 4.510, 4.473 and 4.459 for x = 0.0, 0.1 and 0.2, respectively.

Furthermore, according to the statistical theory, the three critical exponents obey the Widom scaling relation [23]:

$$\delta = 1 + \frac{\gamma}{\beta} \tag{7}$$

Using this equation, δ values are calculated with β and γ values obtained from the modified Arrott plot and from the KF method (see in Table 1). The values obtained from critical isotherms M (T_C, $\mu_0 H$) are close to those determined with the Widom scaling relation, which implies that the obtained β and γ values are consistent. At this level, the obtained critical exponents values can be verified with the prediction of the scaling theory in the critical region using this equation:

$$M(\mu_0 H, \varepsilon) = \varepsilon^{\beta} f \pm \left(\frac{\mu_0 H}{\varepsilon^{\beta+\gamma}}\right) \tag{8}$$

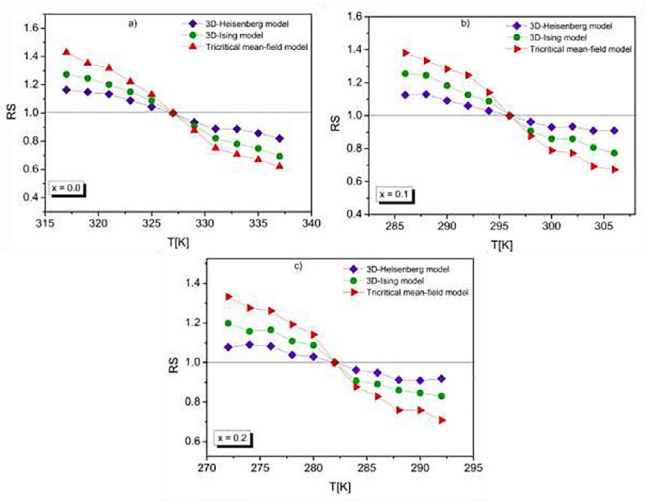

Fig. 5. . Relative slope (RS) as a function of temperature for (a) x = 0.0 (b) x = 0.1 and (c) x = 0.2.

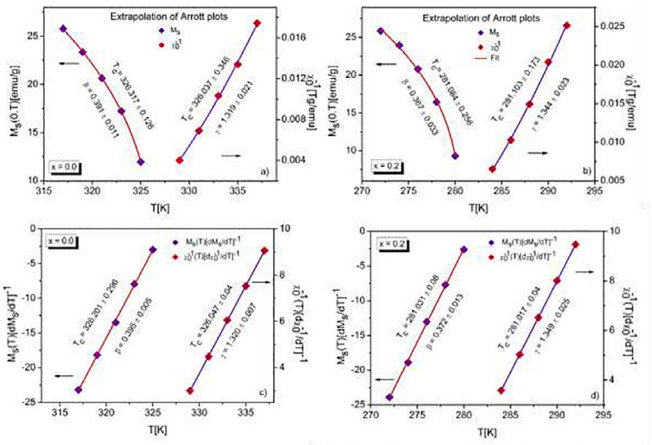

Fig. 6. (a) and (b) Temperature dependence of spontaneous magnetization (M_S(T. 0) and inverse initial susceptibility χ_0^{-1}(T) for x = 0.0 and x = 0.2, respectively. (c) and (d) Kouvel – Fisher plots of $M_S(T)\left[\frac{dM_S(T)}{d(T)}\right]^{-1}$ and

Where (f+) and (f−) are used for above and below T_C, respectively [24].

Taking the values of β, γ and T_C from the KF method, the scaled data $M|\varepsilon|^{-\beta}$ vs. $\mu_0 H|\varepsilon|^{-(\beta+\gamma)}$are plotted in Fig. 8a and b and the logarithmic scale in Fig. 8 c and d for x = 0.0 and 0.2, respectively. It can be clearly seen that all the points fall on two curves, one for $T < T_C$ and another for $T > T_C$. Both scaling results confirm that the critical parameters of our compounds are pretty well consistent with the scaling hypothesis, strongly prove corroborates the reliability of the obtained critical exponents. We can note that the scaling is good at high fields, it becomes poor at low fields below T_C. This could be ascribed to the magnetic inhomogeneities and the effect due to the uncertainty in the calculation of the demagnetization factor, which becomes considerable in this region [25].

4. Conclusion

To conclude, a detailed investigation of the critical behavior of $Ni_{0.3-x}Cu_xZn_{0.7}Fe_2O_4$ (x = 0.0, 0.1 and 0.2) spinel ferrites has been carried out. The systematic crystal structure of $Ni_{0.1}Cu_{0.2}Zn_{0.7}Fe_2O_4$ (x = 0.2) compound is generated using output.cif file by VESTA program, which indicates that the structure is well described with the cubic spinel with the general formula AB_2O_4. From the SEM analysis, our materials have an irregular morphology (spherical, polygonal, cubic) and the diameters of particles were 600–642 nm. These spinel ferrites undergo a second order ferromagnetic–paramagnetic transition. It is noted that the introduction of Cu ion in octahedral B-sites of Zn-Ni spinel ferrite does not alter the universality class, where the estimates critical exponents (β, γ and δ) values are close to those theoretically predicted for the 3D-Heisenberg model. The field and temperature dependent magnetization follows the scaling theory, and all data fall on two distinct branches, one for $T < T_C$ and another for $T > T_C$, indicating that the critical exponents obtained in this work are accurate.

Declaration of Competing Interest

The authors declare that they have no known competing financial interests or personal relationships that could have appeared to influence the work reported in this paper.

Acknowledgements

The Tunisian Ministry of Higher Education and Scientific Research for supported this work.

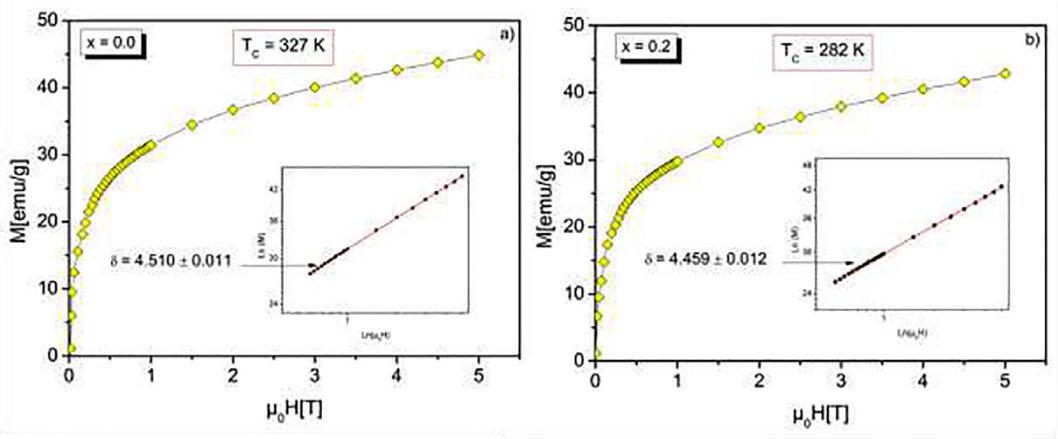

Fig. 7. Critical isotherm of M vs. μ_0H close to the Curie temperature for (a) x = 0.0 and (b) x = 0.2. Insets shown the same on logarithmic scale and the straight line is the linear fit following Eq. (3). The critical exponent δare obtained from the slope of the linear fit.

Table 1
Comparison of critical exponents of $Zn_{0.7}Ni_{0.3-x}Cu_xFe_2O_4$ (x = 0.0, 0.1 and 0.2) compounds with earlier reported data, and with the various theoretical models. Abbreviations: CI, critical isotherm; MAP, modified Arrott plots and KF, Kouvel–Fisher.

Composition	Method	T_C(K)	β	γ	δ	References
$Ni_{0.\ 3}Zn_{0.7}Fe_2O_4$	MAP	326.317	0.391	1.319	4.373	**This work**
	KF	326.201	0.395	1.320	4.341	
	CI				4.510	
$Ni_{0.2}Cu_{0.\ 1}Zn_{0.7}Fe_2O_4$	MAP	295.662	0.384	1.321	4.440	**This work**
	KF	296.050	0.386	1.329	4.443	
	CI				4.473	
$Ni_{0.1}Cu_{0.2}Zn_{0\ .7}Fe_2O_4$	MAP	281.084	0.367	1.344	4.662	**This work**
	KF	281.031	0.372	1.349	4.626	
	CI				4.459	
Mean field	theory		0.5	1	3	[13]
3D-Heisenberg	theory		0.365	1.336	4.80	[13]
3D-Ising	theory		0.325	1.24	4.82	[13]
Tricritical mean field	theory		0.25	1	5	[13]
$NiFe_2O_4$		865.4	0.378	1.330	–	[21]
$Zn_{0.5}Ni_{0.5}Fe_2O_4$		553.5	0.442	1.386	–	[21]
$Zn_{0.75}Ni_{0.25}Fe_2O_4$		295.2	–	1.420	–	[21]
Fe_3O_4		853.8	0.379	1.345	–	[21]
$Zn_{0.2}Fe_{2.8}O_4$		763.5	0.40	1.35	–	[22]
$Ni_{0.6}Cd_{0.2}Cu_{0.2}Fe_2O_4$		681.6	0.403	1.073	3.650	[9]

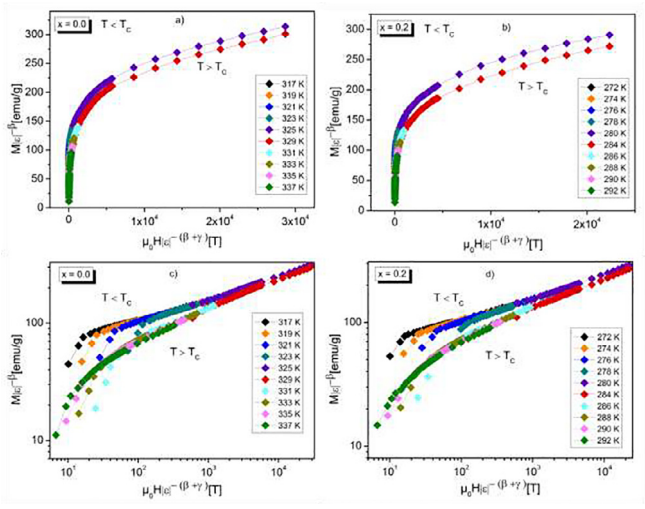

Fig. 8. Scaled magnetization for (a) x = 0.0 and (b) x = 0.2 below and above T_C, using β and γ mentioned in the text. (c) and (d) shown the same plot on a logarithmic scale. These plot shows that all the data collapse onto two different curves: one below T_C and another above T_C.

Appendix A. Supplementary data

Supplementary data to this article can be found online at https://doi.org/10.1016/j.jmmm.2020.166531.

References

[1] E. Melagiriyappa, H.S. Jayanna, Structural and magnetic susceptibility studies of samarium substituted magnesium–zinc ferrites, J. Alloy. Compd. 482 (2009) 147.
[2] Alex Goldman, Modern Ferrite Technology, second ed., Springer, New York, 2006.
[3] E. Sagar, R.H. Kadam Shirsath, Anil S. Gaikwad, Ali Ghasemi, Akimitsu Morisako, Effect of sintering temperature and the particle size on the structural and magnetic properties of nanocrystalline $Li_{0.5}Fe_{2.5}O_4$, J. Magn. Magn. Mater. 323 (2011) 3104.
[4] D.H. Bobade, S.M. Rathod, Maheshkumar L. Mane, Sol–gel auto-combustion synthesis, structural and enhanced magnetic properties of Ni^{2+} substituted nano-crystalline Mg–Zn spinel ferrite, Phys. B. 407 (2012) 3700.
[5] Elaa Oumezzine, Sobhi Hcini, Mohamed Baazaoui, E.K. Hlil, Mohamed oumezzine, critical behavior of $Zn_{0.6-x}Ni_xCu_{0.4}Fe_2O_4$ ferrite nanoparticles, J. Alloys. Compd. 656 (2016) 676.
[6] M.S. Anwar, Faheem Ahmed, Bon Heun Koo, Enhanced relative cooling power of $Ni_{1-x}Zn_xFe_2O_4$ ($0.0 \leq x \leq 0.7$)) ferrites, Acta Mater. 71 (2014) 100.
[7] D.P. Shahida Akhter, S.M. Paul, M.A. Hoque, M. Hakim, R. Hudl, P. Nordblad Mathieu, Magnetic and magnetocaloric properties of $Cu_{1-x}Zn_xFe_2O_4$ (x = 0.6, 0.7, 0.8) ferrites, J. Magn. Magn. Mater. 367 (2014) 75.
[8] S. Hcini, N. Kouki, A. Omri, A. Dhahri, M.L. Bouazizi, Effect of sintering temperature on structural, magnetic, magnetocaloric and critical behaviors of Ni-Cd-Zn ferrites prepared using sol-gel method, J. Magn. Magn. Mater. 464 (2018) 91.
[9] N. Kouki, S. Hcini, M. Boudard, R. Aldawas, A. Dhahri, Microstructural analysis, magnetic properties, magnetocaloric effect, and critical behaviors of $Ni_{0.6}Cd_{0.2}Cu_{0.2}Fe_2O_4$ ferrites prepared using the sol–gel method under different sintering temperatures, RSC Adv. 9 (2019) 1990.
[10] R. Felhi, H. Omrani, M. Koubaa, W. Cheikhrouhou Koubaa, A. Cheikhrouhou, Enhancement of magnetocaloric effect around room temperature in $Zn_{0.7}Ni_{0.3-x}Cu_xFe_2O_4$ ($0 \leq x \leq 0.2$) spinel ferrites, J. Alloy. Compd. 758 (2018) 237.
[11] R. Cabassi, F. Bolzoni, A. Gauzzi, F. Licci, Critical exponents and amplitudes of the ferromagnetic transition in $La_{0.1}Ba_{0.9}VS_3$, Phys. Rev. B: Condens. Matter 74 (2006) 184425.
[12] M. Fähnle, W.U. Kellner, H. Kronmüller, Use of scaling plots in phase-transition studies, Phys. Rev. B Condens. Matter. 35 (1987) 3640.
[13] S.N. Kaul, Static critical phenomena in ferromagnets with quenched disorder, J. Magn. Magn. Mater. 53 (1985) 5.
[14] S. Das, T.K. Dey, Structural and magnetocaloric properties of La1 − yNayMnO3 compounds prepared by microwave processing, J. Phys. D Appl. Phys. 40 (2007) 1855.
[15] C.H.V. Mohan, M. Seeger, H. Kronmüller, P. Murugaraj, J. Maier, Critical behaviour near the ferromagnetic-paramagnetic phase transition in $La_{0.8}Sr_{0.2}MnO_3$, J. Magn. Magn. Mater. 183 (1998) 348.
[16] D. Kim, B. Revaz, B.L. Zink, F. Hellman, J.J. Rhyne, J.E. Mitchell, Tricritical point and the doping dependence of the order of the ferromagnetic phase transition of $La_{1-x}Ca_xMnO_3$, Phys. Rev. Lett. 89 (2002) 227202.
[17] H.E. Stanley, Introduction to Phase Transitions and Critical Phenomena, Oxford University Press, London, 1971.
[18] A. Arrot, J.E. Noakes, Approximate equation of state for nickel near its critical temperature, Phys. Rev. Lett. 19 (1967) 786.
[19] J. Fan, L. Ling, B. Hong, L. Zhang, L. Pi, Y. Zhang, Critical properties of the perovskite manganite $La_{0.1}Nd_{0.6}Sr_{0.3}MnO_3$, Phys. Rev. B 81 (2010) 144426.
[20] S. Kouvel, M.E. Fisher, Detailed magnetic behavior of nickel near its curie point, Phys. Rev. 136 (1964) A1626.
[21] M. Haug, M. Fahnle, H. Kronmuller, F. Haberay, Phase transitions in ordered and disordered ferrimagnets. II. Experimental results, Phys. Status Solidi 144 (1987) 411.
[22] C.J. Tinsley, Magnetic critical point behaviour of magnetite and related ferrite spinels, J. Magn. Magn. Mater. 15 (1980) 459.
[23] B. Widom, Surface tension and molecular correlations near the critical point, J. Chem. Phys. 43 (1965) 3892.
[24] S. Murakami, N. Nagaosa, Colossal magnetoresistance in manganites as a multi-critical phenomenon, Phys. Rev. Lett. 90 (2003) 197201.
[25] R. Li, C. Zhang, L. Pi, Y. Zhang, Tricritical point in hole-doped manganite $La_{0.5}Ca_{0.4}Li_{0.1}MnO_3$, Europhys. Lett. 107 (2014) 47006.